CONCRETE LIBRARY OF JSCE NO. 26, DECEMBER 1995

# ULTIMATE STRENGTH AND FAILURE MECHANISM OF PC MEMBERS UNDER COMBINED AXIAL TENSILE FORCE AND FLEXURE

(Translation from Proceeding of JSCE, No. 508/V-26, February 1995)




Kenji KOSA Kazuo KOBAYASHI Nobuhiko MORITA Shu KANAUMI

Many new prestressed concrete (PC) structural types have recently been developed, and some of them are characterized by the ultimate strength and failure mode which are controlled by a combination of axial tensile force and flexure. To investigate the response of PC members under such loading, experimental studies are first carried out on a box girder bridge with partially prestressed concrete cable stays as a prototype model structure. Next, nonlinear analysis is performed applying a tension stiffening model of concrete to allow a comparison with the experimental results and then evaluate the tension stiffening effect. Finally, using this same model, nonlinear analysis is performed to evaluate the effects of redistribution of internal forces and tensile stiffness on the ultimate strength of the overall structure.

***Keywords*** : *nonlinear analysis, PC, tension, tension stiffness, load-deformation*

---

Kenji Kosa, a member of the JSCE and ASCE, is a senior highway engineer at the Hanshin Expressway Public Corporation, Osaka, Japan. He obtained his Ph.D. from the University of Michigan, Ann Arbor in 1988. His main research interests are the analysis and design of concrete structures.

---

Kazuo Kobayashi is a professor in the Department of Civil Engineering at the Osaka Institute of Technology. He obtained his Dr. Eng. from Kyoto University in 1973 and is the author of several books and many technical papers. His present main research interests are the analyses of prestressed concrete structures. He is a member of the JSCE.

---

Nobuhiko Morita is a manager at the Kansai Branch of Oriental Consultants Co., Ltd. He obtained his BS in civil engineering from Ritsumeikan University in 1980. His research interest is the design of concrete structures. He is a registered consulting engineer and a member of the JSCE.

---

Shu Kanaumi is a manager at Kokusai Structural Engineering Corp. He received his BS in civil engineering from Ritsumeikan University. His research interests are nondestructive testing and the durability design of concrete structures. He is a member of the JSCE.

---

## 1. INTRODUCTION

To date, a number of experimental and analytical studies have been conducted on the behavior of PC members subjected to axial compressive force and flexure. As a result, procedures for the evaluation of their load bearing and deformation behavior are substantially established. On the other hand, very few studies have been carried out on the behavior of PC members subjected to axial tensile force and flexure. The few applications of PC members under such conditions and the difficulties associated with experiments -- great complexity and the large scale required -- seem to be the cause of this paucity of research efforts. However, with the advent of new bridge types of PC structures in recent years, the number of structures in which the ultimate state of members is determined predominantly by the axial tensile force, although affected primarily by the compressive forces at the serviceability state, is increasing. Among structures of this type are PC box girder bridges with diagonal stays, PC truss bridges, and suspended slab bridges. In these structures, PC members would fail after all or almost all of their sections enter the tensile range at the ultimate state. Given the increasing use of such structures, there is an urgent need for exhaustive investigations into the behavior of PC members subjected to this type of loading. This study is part of the effort to meet this need.

The following are representative investigations made in the past with regard to the load bearing and deformation behavior of PC members subjected to axial tensile force:

1) Evaluation of deformation behavior under axial tensile force
For PC members with nonlinear deformation behavior subjected to axial tensile force, it is generally difficult, both experimentally and analytically, to evaluate the complex decline in tensile stiffness that accompanies the formation of tensile cracks[1) 2)]. Collins et al. attempted to develop a procedure for predicting the relationship between average concrete stress and average concrete strain as follows[3)]. When reinforcing bars embedded in the PC members do not yet yield,

$$\varepsilon_c = \varepsilon_s = N_s \,/\, (A_s \cdot E_s)$$
$$N_s = N - N_c$$
$$N_c = A_c \cdot f_c \qquad (1)$$

where,

$\varepsilon_c$ : Average concrete strain
$\varepsilon_s$ : Average reinforcing bar strain
$N_s$ : Load carried by reinforcing bar
$E_s$ : Young's modulus of reinforcing bar
$N$ : Axial tensile force applied
$N_c$ : Load carried by concrete
$A_s$ : Cross-sectional area of reinforcing bar
$A_c$ : Cross-sectional area of concrete
$f_c$ : Average concrete stress

While reinforcing bar strain remains within the elastic range, it is possible to estimate the share of the load carried by the concrete, by first obtaining the reinforcement-borne load ($N_s$) from the average stain and then subtracting this load from the applied axial force. Collins et al. proposed the following equation for the case $\varepsilon_{cf} > \varepsilon_{cr}$ after considering various existing experimental results:

$$f_c = \alpha_1 \alpha_2 f_{cr} \,/\, (1 + \sqrt{500\ \varepsilon_{cf}}) \qquad (2)$$

where,

$f_c$ : Average concrete stress
$f_{cr}$ : Concrete stress at cracking
$\alpha_1$ : Factor accounting for bond characteristics of reinforcement $(0 \sim 1.0)$

$\alpha_2$ : Factor accounting for characteristics of loading ($0.7 \sim 1.0$)

$\varepsilon_{cf}$ : Average concrete strain

$\varepsilon_{cr}$ : Concrete strain at cracking

However, if a reinforcing bar reaches the yield stress point at any location within the crack plane, the elastic relationship between the average strain and average stress of the bar is lost at that point, even though no yielding can be observed in locations other than this position. In an attempt to deal with this post yield-range, Tamai and Shima et al.[4] used experimental results from pull-out tensile tests of RC bar elements in order to propose a new equation to express the average stress-strain relationship of concrete beyond the yield point. Based on the results of the tests, they assumed that the stress distribution in the reinforcement draws a cosine curve and also the tensile stiffness of the concrete remains unchanged even after the yield point of a bar is reached.

2) Evaluation of shear strength under axial tensile force

In evaluating the shear strength of a member subjected to axial tensile force utilizing the design shear strength equation based on the "addition law" that is consisted of concrete contribution and shear reinforcement contribution in the "Standard Specifications for Concrete Structures by Japan Society of Civil Engineers (JSCE Concrete Specifications)," it is generally recognized that two types of decline in shear-carrying capacity should be taken into consideration. One is the decline in the shear resistance of the concrete due to the action of the axial tensile force, and the other is the decline in the shear resistance carried of the web reinforcements because cracks are likely to propagate not at 45° to the axial tensile force, but perpendicular to it. Therefore, the latest version of the specifications [5] requires that the safety against shear strength be increased by applying the equation $\beta_n = 1 + 2\, M_o / M_d$, which derives from the experimental results of Haddadin et al. ( $\beta_n$ : factor accounting for the contribution of axial force to the shear strength; $M_d$ : design bending moment; $M_o$ : bending moment at the decompression state of section.) Tamura et al.[6] have also suggested an equation that modifies the design equation given in the "JSCE Concrete Specifications" based on their experimental results. On the other hand, Collins et al. have proposed the so-called Modified Compression Field Theory[7], recognizing from a macroscopic viewpoint that a concrete element with cracks is a continuous element and obtaining its shear strength from the equilibrium and compatibility conditions for average stress and average strain within the given element.

As these examples demonstrate, basic investigations have already been made with regard to the behavior of PC members subjected to axial tensile force. In reality, however, it is extremely rare for axial tensile force alone to act on a PC member, and it is normally joined by a bending moment and other forces. Only a very limited number of studies have so far treated with the behavior of members under a combination of axial tensile force and bending moment.

Hence, by incorporating preceding studies by other investigators into our research, we aimed first to investigate the ultimate strength and failure mechanism of PC members subjected to axial tensile force and bending moment through experiments on a PC box girder bridge with diagonal concrete stays. The ultimate state of this prototype model structure is primarily governed by the axial tensile force. Our experiments were conducted using 1/3-scale specimens of a bridge, and two test parameters were adopted: the ratio of axial tensile force to bending moment and the shear steel ratio. Following this experimental work, we took an analytical approach using the above-mentioned Collins model subjected to axial tensile force, and the results were evaluated to examine the applicability of the analytical model to the loading condition with a combination of axial tensile force and bending moment. Finally, using the material properties with the tension stiffening effect, the nonlinear analysis was extended over the entire bridge structure. And, the redistribution effect as well as the tensile stiffening effect were evaluated by comparing its results with those obtained from the linear analysis.

## 2. STRUCTURE OF THE MODEL BRIDGE (BOX-GIRDER BRIDGE WITH CONCRETE STAYS)

2.1 Features of the bridge

The model bridge is a three-span PC box girder bridge with concrete stays and is 285 m long (75 + 140 + 70). This concrete-stayed bridge is a structure in which the PC members are diagonally connected to an ordinary box girder bridge. This design can be considered to be a special type of a cable-stayed bridge, since it has diagonal stays, in which the height of the main girder section can be reduced due to the truss effect of the diagonal stays. Several advantages might be derived from the use of the PC members as diagonal stays: 1) The diagonal members are protected from corrosion and offer a wind mitigation effect; 2) Fatigue problems are almost eliminated because of the low stress amplitude in the cables; 3) Deformation is expected to remain small because the overall rigidity of the structure should be higher.

From an economical point of view, this bridge design is considered comparable with PC box girder bridges and PC cable-stayed bridges for span lengths of about 100-200 m. One internationally known bridge of this type is the Ganter Bridge in Switzerland. In Japan, the Sanriku Railways Omotogawa Bridge in the Tohoku region is of this type, and another, the Natorigawa Bridge, is being constructed on the JR Tohoku Line by East Japan Railway Co.

When this model bridge with PC stays is designed according to "Specifications for Highway Structures" by Japan Road Association, the height of the main girder can be reduced to as little as 3.5 m at the central span and 2.5 m at the side spans, which is an enormous reduction compared with the mid-span height of 8 m for an ordinary box girder bridge. A further benefit is that the bending moment of 18,000 tf · m at the intermediate support due to the dead load will be offset by 8,000 tf · m through the prestressing effect of the diagonal stays, and a further 7,000 tf · m or so can be offset by the compressive force resulting from the truss effect of the stays. Focusing on the stresses in the cross section, a compressive stress of 37 kgf/cm$^2$ together with a positive bending stress of 48 kgf/cm$^2$ will act against the tensile stress of 108 kgf/cm$^2$ caused by the dead load bending moment. On the other hand, as for the bending moment acting on the diagonal stays in the axial direction of the bridge, a section where a stay intersects a main pylon will have a higher moment than a section where a stay intersects a main girder, as shown in Fig. 2. Furthermore, a cross section of the stay on the pylon side (150 x 80 cm) is smaller than that on the girder side (350 x 50 cm), which means a higher stress will be imposed on the pylon side than on the girder side. As a result, more careful consideration is needed for the pylon side section than for the girder side. However, this structure is extremely advantageous as regards the stress-fatigue problem, because the stress on the pylon side is (at most) 3 kgf/mm$^2$, being considerably small compared with the value of 10 kgf/mm$^2$ in the case of an ordinary cable-stayed bridge. The diagonal cables needed for a concrete stay are four 720 T type (27S15.2) to withstand the total design load acting after its completion.

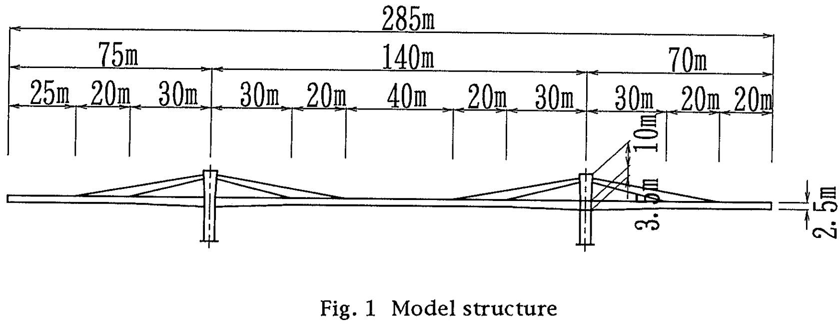


Fig. 1 Model structure

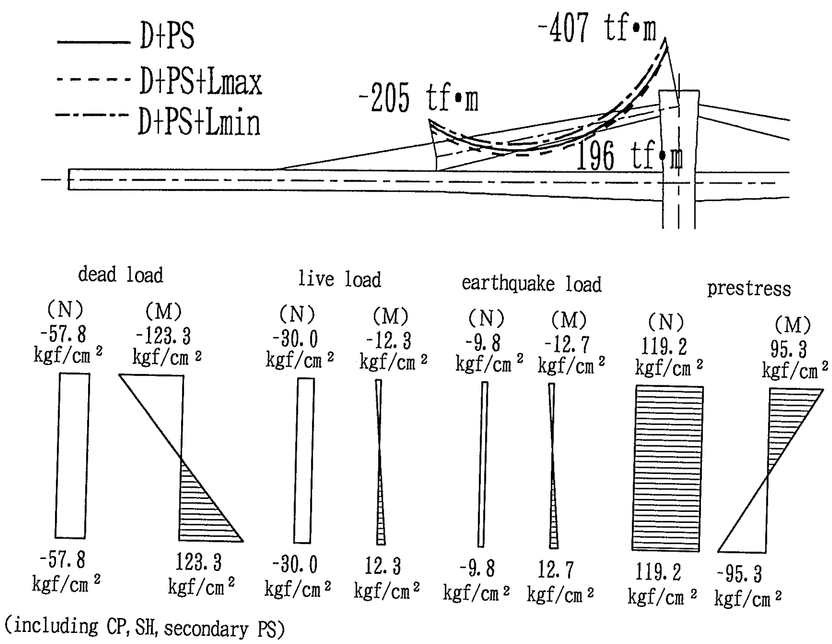


Fig.2 Cross Sections of diagonal stay and their stresses

## 2.2 Simple analysis of load bearing capacity

In order to examine roughly the load bearing characteristics of this concrete-stayed bridge which is designed in accordance with the "Specifications for Highway Bridges", the resisting bending moments were calculated for several sections, and then they were used in an estimation of how much safety will be available beyond the design load. For that purpose, the interaction curve of axial force vs. bending moment (N-M curve) at the ultimate state of these sections was plotted as well as a plot of sectional forces (N, M) derived from a linear frame analysis of the entire structure in which the stiffness was kept constant at each step of load increase. The point where the two lines cross was defined as the failure load, and the load factor at that point was extracted. Figure 3 shows the cross sections considered. Table 1 gives the safety factors of the members. Figure 4 is the N-M interaction curve at the intersection of a stay and a main pylon.

As shown in Table 1, as for the $D + \alpha L$ (an investigation to determine by how much the bearing capacity exceeds the design live load when the design dead load is constant), the safety factor $\alpha$ was 6.7 at the intersection of a stay and a girder, while it was 5.3 at the intersection of a stay and a pylon. This indicates that the latter is the most critical section. Further, as for the $\beta (D + L)$ (an investigation to determine by how much the bearing capacity exceeds the design dead load plus the design live load), although the safety factor dropped to a relatively small 3.2 at the intersection of a pylon and a main girder, it was 2.5 at the intersection of a stay and a main pylon. Again, this points to the latter being the most vulnerable section. As seen in Fig. 4, which shows the N-M interaction curve at the intersection of a stay and a pylon, the axial tensile force increases with increasing loading in both $D + \alpha L$ and $\beta (D + L)$, and the failure occurs when the bottom fiber of the section reaches the ultimate compressive strain of concrete. However, as stated earlier, investigations so far are inadequate with regard to the behavior of PC members subjected to predominant tensile axial loading. Therefore, the ultimate strength of planned bridge and the reliability of the design procedure is examined through experiment in the next section.

Table. 1 Safety factor of members

| Member No. | | α | β |
|---|---|---|---|
| Main girder | ① | 14.4 | 4.1 |
| | ② | 9.1 | 3.2 |
| | ③ | 6.7 | 3.6 |
| | ④ | 14.0 | 3.7 |
| Diagonal stay | Ⓐ | 5.8 | 2.6 |
| | Ⓑ | 5.3 | 2.5 |
| | Ⓒ | 5.3 | 2.8 |

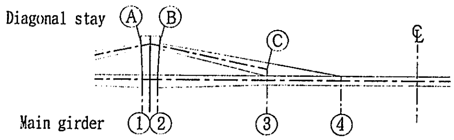

Fig.3 Cross section used calculating safety factor

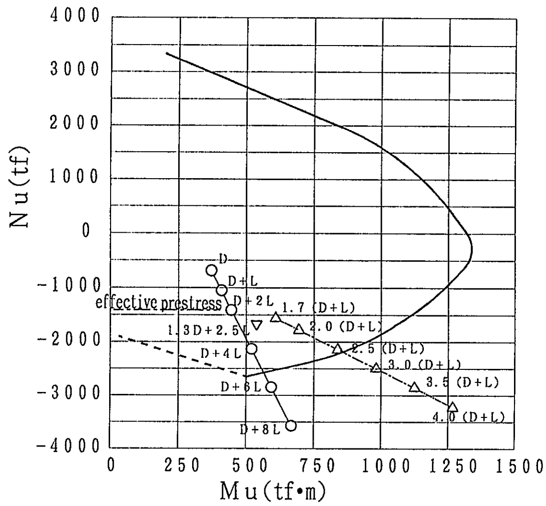

Fig. 4 Axial force-moment(N-M)curve at intersection of diagonal stay and pylon

## 3. EXPERIMENTAL EVALUATION OF LOAD BEARING BEHAVIOR

### 3.1 Objectives

The objectives of experimental investigation related to the behavior of PC members subjected to combined tensile axial force and bending moment are itemized below.

1) Load bearing capacity under axial tensile force and bending moment
The ratio of axial tensile force to bending moment may affect the behavior of members in the ultimate state, and then this ratio was adopted as a parameter in the experiment. As shown in Fig. 5, three load combinations were applied to the cross section of PC members in which high compressive stress had been introduced in advance by prestressing. The first was a loading type with small increase in tensile axial force and large increase in bending moment ($\beta$ $(D + L)$ where $\beta$ = load factor, $D$ = dead load, $L$ = live load). The second was a type with large increase in tensile axial force and small increase in bending moment ($D + \alpha L$ where $\alpha$ = load factor). The final type of loading comprised an increase in tensile axial force alone.

2) Deformation behavior
Under the action of axial tensile force, the load elongation behavior ($N$-$\varepsilon$ relation) of the members will be greatly affected by the development of cracks and by the reinforcing bar pull-out behavior. And also the analysis of the ultimate behavior of the entire structure system will be significantly influenced by the deformation performance of the members in addition to their load bearing capacity. The experiment thus was conducted to examine the deformation behavior of the members, $N$-$\varepsilon$ relationship, that would change with variations in loading.

3) Shear strength under axial tensile force
When shear cracks form, they propagate diagonally in a direction perpendicular to the member axis due to axial tensile force, resulting in reducing shear strength. Therefore, to determine the shear strength of the members under axial tensile force, three cases were compared, each with a different shear reinforcement ratio. The first corresponded to the required shear reinforcement ratio for an actual bridge as determined from shear and torsion. The second took only the design shear force into

consideration. The third considered the minimum reinforcement ratio designated in the Japanese "Specifications for for Highway Bridges."

### 3.2 Preparation of specimens

As shown in Table 2, five specimens were produced for the investigations described above. These specimens were designed to have a configuration representing the actual box girder bridge with diagonal stays being designed to 1/3 scale. The sectional area of 800 x 1500 mm in the real bridge at the intersection of a stay and a pylon was reduced to 250 x 500 mm in the specimens. The height of the specimen column was made 3 m, which is approximately six times the depth of cross section, so that the development of cracks and deformation behavior could be adequately tested. To introduce the prestress, two F130T prestressing steel bars were placed in the column according to the SEEE method. The bottom end of the column was made a dead anchor and the jacking force was applied at the top face. The eccentricity of prestressing steel was determined to be 6.7 cm. Prestress was applied to the upper fiber of the cross section at an intensity of 219 kgf/cm$^2$ and to the bottom fiber at 23 kgf/cm$^2$ to achieve a stress distribution roughly identical to that of the actual bridge. As to the shear reinforcing bars, D10 bars were placed in the specimens at three different spacings of 100, 150, and 200 mm throughout the full height of the column to comply with the three test cases. Table 3 shows the physical properties of the five specimens.

### 3.3 Load application and measurements

Figure 7 outlines the loading equipment. The specimen was placed horizontally within the loading frame and the bottom end of the column was anchored in the lower end of the frame using PC steel bars ($\phi$ 32 mm). Axial tensile force was introduced by prestressing another PC steel bars embedded in the upper end of the specimen. Horizontal force was applied using a hydraulic jack. The direction in which the axial tensile force acts was adjusted in accordance with the deformation of the top end of the column so as to maintain correspondence with the longitudinal axis of the specimen. As to the loading procedure, the axial load was applied first, in principle, followed by the horizontal load, as shown in Fig. 5. Taking this as one cycle, the axial force was increased with an increment of 20 tf up to $N$ =140 tf, and after that at an increment of 10 tf until the ultimate load was reached. Measurements were taken up to a height of 2 m from the bottom end, concentrating near the bottom end. Measurements consisted of concrete surface strain, longitudinal steel strain, stirrup strain, applied load, and horizontal and vertical displacement.

### 3.4 Experimental results

In these experiments, the ultimate state was assumed to have been reached when any of the following conditions were met from a viewpoint of safety in these large-scale tests.

1) At the point when the maximum concrete compressive strain reached approximately 3,000 $\mu$ (90% of the ultimate compressive strain specified in "Specifications for Highway Bridges".)

2) At the point when total tensile strain (effective strain plus measured strain due to applied load) in the PC steel reached nearly 12,000 $\mu$ (0.2% strength of the F130T PC steel).

3) At the point when PC members lost their innate function due to cracks extending throughout the specimen.

Although the specimens were expected to fail in shear, the observed failure modes were all of the flexural type. Here, taking the No. 2, 3, and 4 specimens as representative of the different loading combinations, the experimental results are explained.

1) No. 2 specimen

A first crack appeared at the bottom of the column when the axial force reached 150 tf. Subsequently, cracks appeared at a position 30 cm from the bottom (section A-A in Fig. 6) when the axial force reached 160 tf and at positions 15 and 60 cm from the bottom when the force was 170 tf (Fig. 9). When the axial force reached 207 tf together with bending moment of 28.6 tf · m, the total strain in PC steel was 11,650 μ and the crack width at the bottom widened up to 3 mm, causing a flexural failure.

2) No. 3 specimen
A first crack arose at the bottom of the specimen when the axial force reached 167 tf. Cracks occurred at a location 20 cm from the bottom when the axial force reached 187 tf and at locations 40 and 50 cm from the bottom when the force was 197 tf. A further crack appeared at a point 70 cm above the bottom when the force was increased to 207 tf. Although all cracks propagated roughly in the horizontal direction, it was judged that the ultimate state had been reached when the last crack (70 cm from the bottom) penetrated finally through the entire section at an axial force of 226 tf. At that time, 26,000 μ of tensile strain was observed in the longitudinal reinforcing bars around the bottom of the specimen.

3) No. 4 specimen
Cracks first appeared at positions 1.0 m and 1.5 m from the bottom of the specimen, quite different from the first appearance in other specimens, when the axial force reached 100 tf. Cracks increased in number with increasing axial force, and the specimen was judged to have reached the ultimate state when the total strain of the PC steel attained 12,5000 μ at the axial force of 232 tf. The average crack spacing was about 20 cm at that loading level.

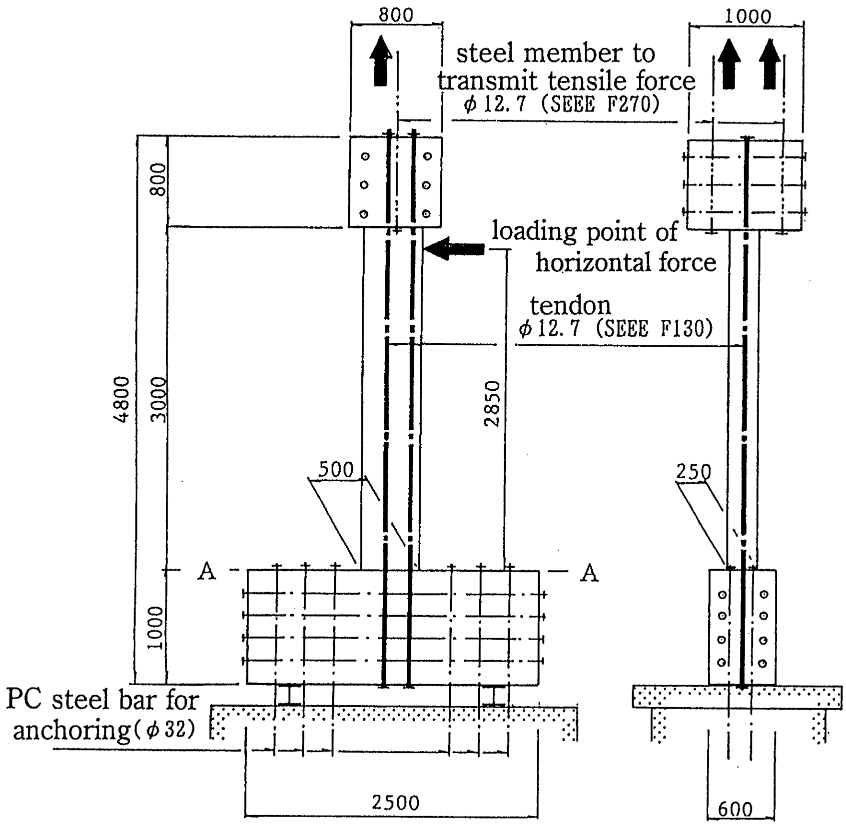


Fig.6 Specimen for loading test

Table 2 Combination of experimental atributes

| specimen No. | loading type | PC steel bar | shear reinforcement | | |
|---|---|---|---|---|---|
| | | | reinforcing method | stirrup | reinforcement in the axial direction |
| No.1 | low axial force | 2-F130T | minimum shear reinforcement | D10@200mm | 4 bars-D10 |
| No.2 | low axial force | 2-F130T | shear reinforcement only | D10@150mm | 6 bars-D10 |
| No.3 | high axial force | 2-F130T | current design | D10@100mm | 10 bars-D10 |
| No.4 | axial force only | 2-F130T | current design | D10@100mm | 10 bars-D10 |
| No.5 | low axial force | 2-F130T | current design | D10@100mm | 10 bars-D10 |

(Note 1) High axial force is a load combination equivalent to D + $\alpha$ L.
(Note 2) Low axial force is a load combination equivalent to $\beta$ (D + L).
(Note 3) Axial force only means only tensile force is added as external force.
(Note 4) Current design means to position reinforcements to resist torsional and shear forces.

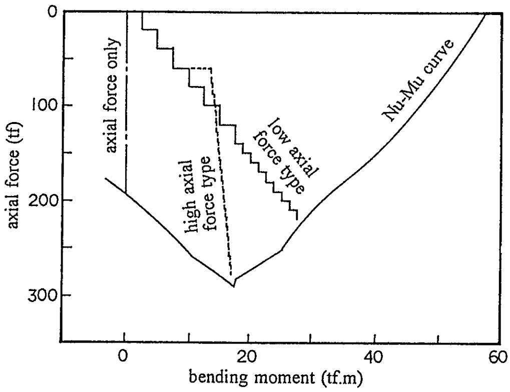


Fig.5 Load path

Table 3 Properties of materials used

test results on properties of concrete used for specimens

| specimen No. | compressive strength (kgf/cm $^2$ ) | static modulus of elasticity (kgf/cm $^2$ ) | tensile strength (kgf/cm $^2$ ) | flexural strength (kgf/cm $^2$ ) |
|---|---|---|---|---|
| No.1 | 605 | 360,000 | 45 | 58 |
| No.2 | 597 | 349,000 | 39 | 66 |
| No.3 | 618 | 380,000 | 42 | 69 |
| No.4 | 500 | 325,000 | 40 | 60 |
| No.5 | 514 | 370,000 | 37 | 62 |

test resutls on properties of PC steel bars used for specimens (SWPR7B)

| tensile strength (kgf/mm $^2$ ) | yield strength (kgf/mm $^2$ ) | modulus of elasticity (kgf/mm $^2$ ) | elongation (%) |
|---|---|---|---|
| 200 | 171.20 | 19,400 | 6.7 |

## 4. ANALYSIS FOR THE EVALUATION OF LOAD-BEARING BEHAVIOR

### 4.1 Evaluation of ultimate strength and the N-M curve

a) Method of analysis

Numerical analysis was carried out to evaluate the ultimate load bearing capacity under the action of axial tensile force and bending moment. The flow chart in Fig. 10 indicates the process in analysis. An integrated strain distribution in the cross section was first obtained by incorporating the strain distribution due to effective prestress with that due to load ($N$, $M$). When this integrated strain distribution satisfies any of the following conditions, it is defined as a failure of the PC members, and the results were compared with the experimental results. The conditions are as follows:

1) When the concrete compressive strain reaches 3,500 $\mu$.
2) When the tensile strain of the PC steel reaches 6.7%.
3) When the reinforcing bar strain reaches 20%.

Figure 11 shows the stress-strain relationship of the constitutive materials used in the analysis. As to the compressive stress-strain curve for the concrete, the curve specified in Japanese "Specifications for Highway Bridges" was chosen for the present analysis from among the various equations that take the softening range in the falling branch region into account. This curve was adopted because, in general, the softening range does not give significant influence on the ultimate strength of specimens. Regarding the method of evaluating load bearing capacity, there were two alternatives: one was to be based on the ultimate strain of the materials, and the other the maximum bending moment under a given axial force. Although a comparison of these two methods is presented in Fig. 12, the simpler and more handy former method was adopted here, because the difference between the methods was relatively small. Also, under axial tensile loading, tensile stiffness of concrete is presumed to give influence on the behavior of the members. Therefore, the previously mentioned equation proposed by Collins et al. , which is readily applicable to PC members, was adopted as a model to express the tensile stress-strain relationship of the concrete, along with the following factors:

$\alpha_1$ : Factor accounting for bond characteristics of steels (deformed reinforcing bars: 1.0; prestressing steel strands (bonded) : 0.7)

$\alpha_2$ : Factor accounting for loading type (short-term monotonic loading : 1.0)

$\varepsilon_{ct}$ : Concrete strain at $\sigma = f_{ct}$

b) Results of analysis

Figure 12 shows the results for specimens No. 1, 2, 3, and 4. Also shown in the figure is the ($N$, $M$) loading point, which was calculated utilizing both the concrete compressive strain and the tensile strain of PC steel at the time of the ultimate state in the experiment. The analytical result for specimen No. 2 in Fig. 12 is well in agreement with the experimental one, in which both are in the range where the ultimate state is governed by the compressive failure of concrete at the bottom end. In the No. 3 specimen, loading intensity was to increase toward B point in the figure, but the actual loading path was slightly different from the estimated path near the ultimate state due to the occurrence of a secondary moment. However, the analytical value shows good quantitative agreement with the experimental one. Specimen No. 4 is the case where only axial tensile force was applied. A resultant moment of about 15 tf occurred at the bottom of the column specimen, because the axial loading apparatus restrained the deformation resulting from the moment caused by eccentricity between the loading point and the centroid of the cross section of the member. Analytical value modified to correct this is shown in Fig. 12, which indicates that the analytical result agrees relatively well with the experimental one.

### 4.2 Evaluation of horizontal deformation behavior

a) Method of analysis

The curvature distribution and the horizontal deformation under axial tensile force and bending moment were obtained by an analytical approach and compared with the experimental results. Firstly, strains at the upper and lower fibers of cross section were obtained from the prestressing force and the sectional forces ($N$, $M$) due to applied load. Next, the strain due to loading was derived by deducting the strain due to prestress from these values, and then the curvature ($\phi$) was calculated. Finally, the horizontal deformation ($\delta$) was estimated by integrating the curvature ($\phi$).

b) Results of analysis

Figure 13 shows typical curvature distributions near the ultimate state ($N$: about 200 tf) taken from specimens No. 2 and 3. In the case of No. 2 specimen, though large cracks occurred at localized positions and a relatively rapid increase in curvature was observed at those positions, the average distribution of the experimental results agrees reasonably well with the calculation. In the case of Specimen No. 3, cracks were dispersed well and there is good agreement between the calculation and the measurements. Meanwhile, the longitudinal steels pulled out near the bottom of the column specimen (displacement: about 3 mm), causing a significant difference between the experimental result and the calculated result. Figure 14 shows the horizontal displacement at the same loading as in Fig. 13. The calculated value given in Fig. 14 has been compensated for the effect of steel pull-out by treating it as a rotation angle, taking into account the displacement observed over the 5 cm distance from the bottom of the specimen. As a result, the experimental value shows good agreement with the analytical value.

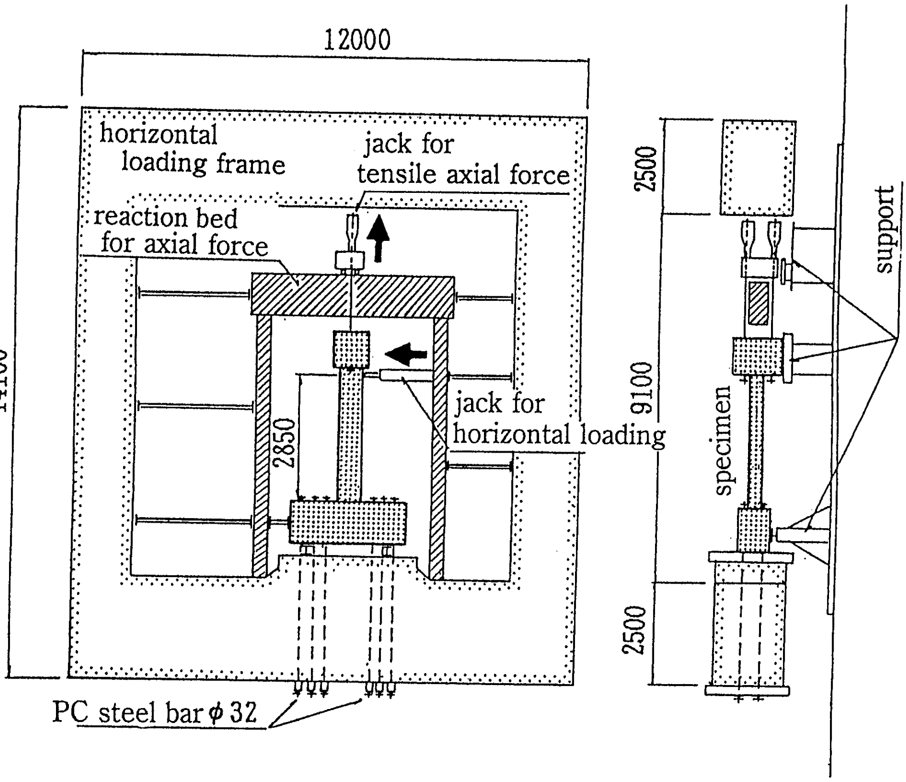


Fig.7 Test setup

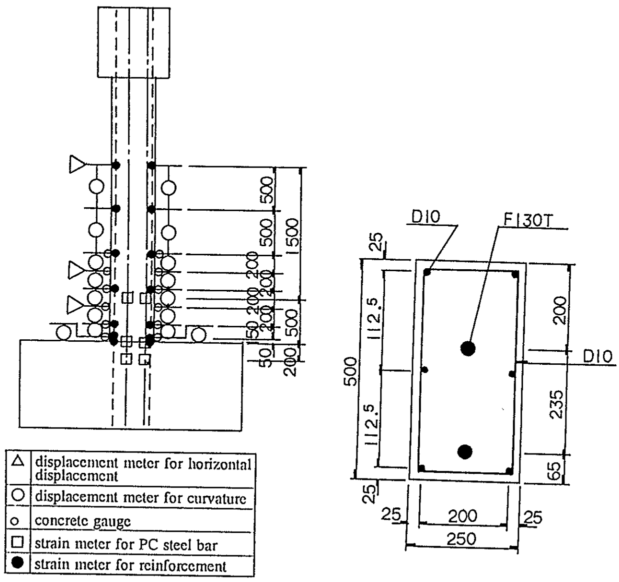


Fig.8 Measuring points and specimen's cross section

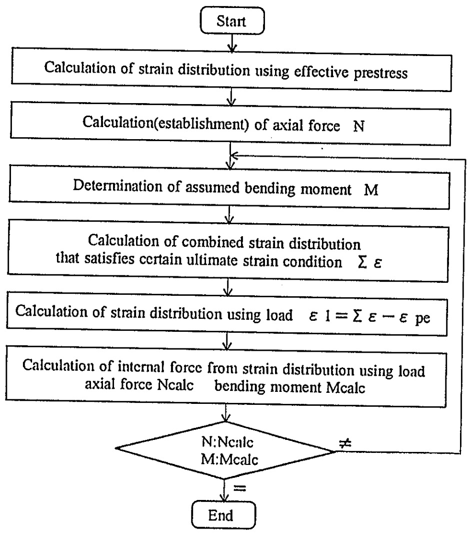


Fig.10 Flowchart for analysis

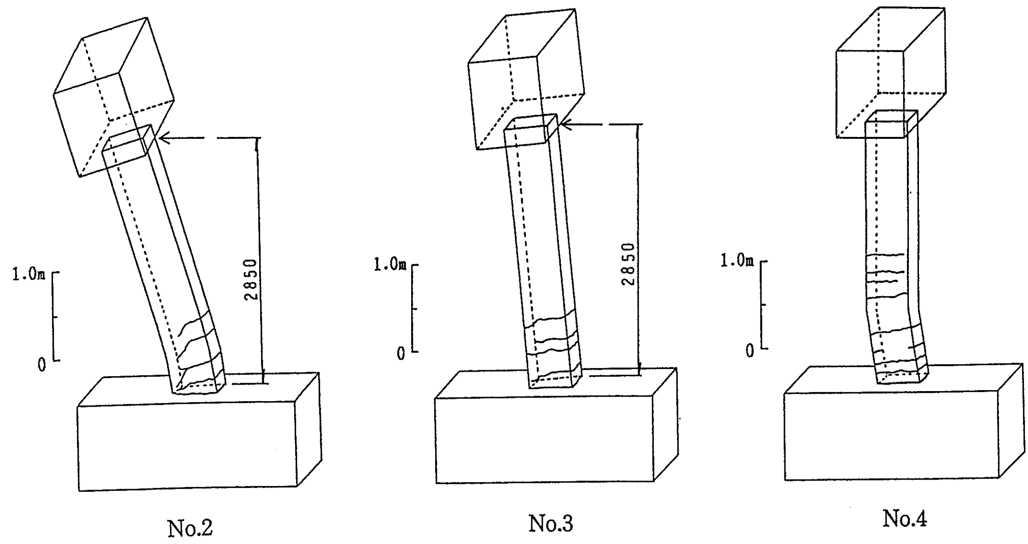


Fig.9 Crack pattern

4.3 Evaluation of deformation in the axial direction under axial tensile force and bending moment

a) Method of analysis

The deformation in the axial direction under the combined axial tensile force and bending moment was obtained analytically and compared with the experimental results. Deformation behavior in the axial direction was evaluated using the average strain derived from the following equations:

$\varepsilon_1$ : Average axial strain by measurement

$(\Sigma \delta_n / L,\ \ \delta_n = (\delta_{n1} + \delta_{n2} / 2)$

$\varepsilon_2$ : Average axial strain by analysis

$(\Sigma \varepsilon_m \triangle x_m / L,\ \ \varepsilon_m = (\varepsilon_{m1} + \varepsilon_{m2} / 2)$

where,

$\delta_{n1}$ , $\delta_{n2}$ : Deformation at upper and lower fibers of cross section over each measured interval.

L: Measurement range

$\varepsilon_{m1}$, $\varepsilon_{m2}$ : Axial strains at upper and lower fibers of cross section within each measured interval.

$\triangle x_m$: Length of each measured interval in the axial direction of column specimen.

The measurement range, L, was made the section between a point 50 mm and a point 2.00 m from the bottom of the specimen, since the pull out of steel reinforcements occurred near the bottom. As to the tensile stiffness of the concrete, two approaches were taken and both sets of results are given in the figures: one was to ignore the stiffness in the softening range, and the other was to take the stiffness in that range into consideration based on the Collins model.

b) Results of analysis

Figure 15 shows the analytical results for specimens No. 1, 2, 3, and 4, which were chosen as representative of the three types of loading outlined earlier (low axial force, high axial force, and axial force only). In the case of specimens No. 1 and 2 (low axial force) , the behavior in the initial stage is in good agreement with the experimental results. Further, in the post-elastic range, the experimental result exists between the analytical ones in which tensile stiffness is considered and not considered. In contrast, in the case of specimen No. 3, the experimental result follows a behavior similar to that where the tensile stiffness is ignored; the gradient of the experimental $N$ - $\varepsilon$ curve on

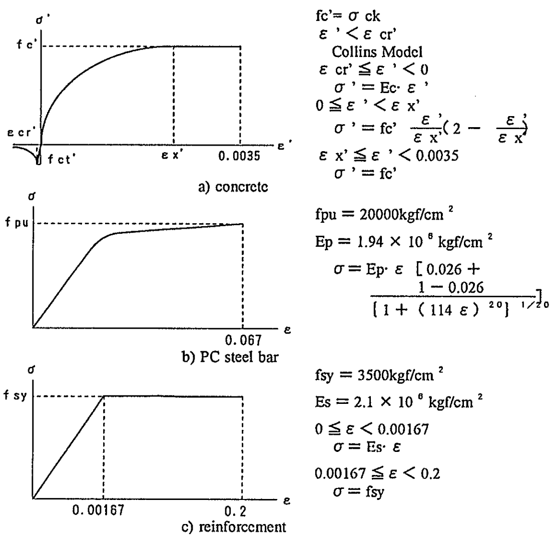


Fig.11 Stress-strain model for materials used

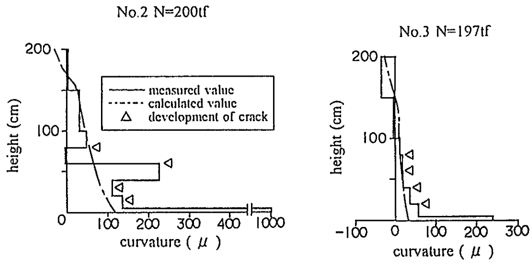


Fig.12 Figure showing N-M correlation

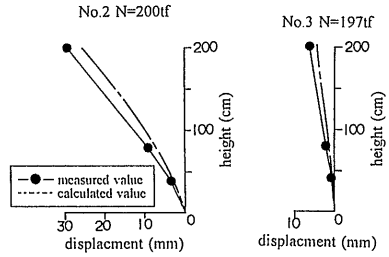


Fig.14 Horizontal displacement

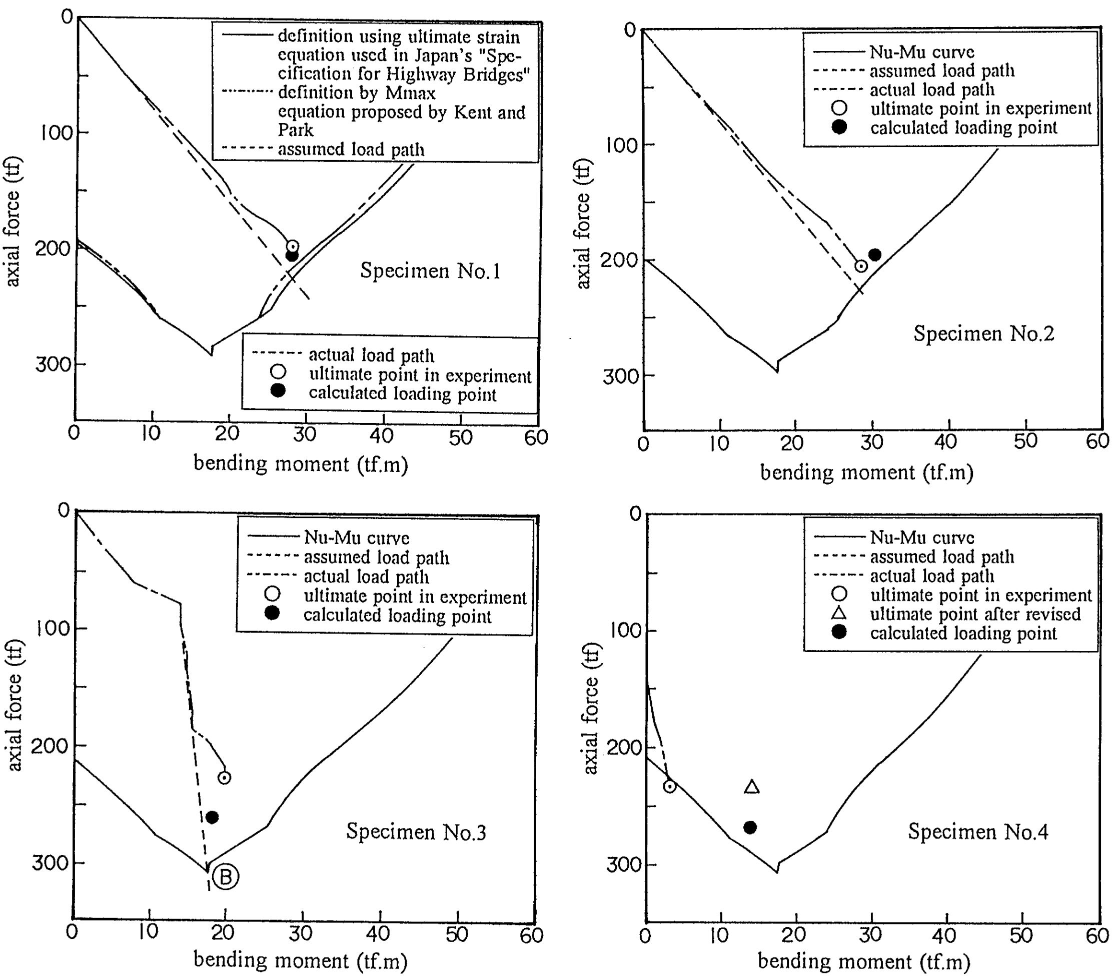


Fig.13 Distribution of curvature

its initial stage is also smaller compared with the analytical one, possibly due to a difference in Young's modulus of concrete between the cylinder test specimen and the column test specimen. When the initial gradient was modified in accordance with the analytical results, the experimental result also exists between the cases where tensile stiffness is considered and ignored. In the case of specimen No. 4, the initial gradient is approximately identical in the experimental and analytical results, and the experimental post-elastic behavior falls between the two analytical cases of tensile stiffness.

It is clear that the experimental results tend to be smaller compared with the analytical results given by the Collins model, which takes tensile stiffness into account. The reason for this is probably that, although the Collins model adopts 0.7 as the bond factor for bonded prestressing strands, the value is smaller in practice due to influences such as grouting condition.

### 4.4 Evaluation of shear strength under the action of axial tensile force

a) Method of evaluation

Collins et at. proposed an analytical method for shear resisting behavior based on the modified compression field theory. This theory does not recognize cracks as individual entities, but rather adopts a macroscopic view and treats concrete component with cracks as continuous elements. These are then analyzed using the equilibrium and compatibility conditions for average stress and average strain within the element. In the Collins model, the shear strength is basically expressed by the following "addition law":

$$V = f_1 b_w jd \cot\theta + (f_v A_v / S)\, jd \cot\theta \qquad (3)$$

where,

$V$ : Shear strength

$f_1$ : Principal tensile stress

$b_w$ : Width of web

$jd$ : Arm length of internal couple

$f_v$ : Average stress in stirrup

$A_v$ : Sectional area of stirrup

$S$ : Spacing of stirrups

$\theta$ : Inclination of cracks

In this equation, the principal tensile stress $f_1$ is determined by the magnitude of principal tensile strain, and the inclination of crack $\theta$ and the stress in stirrup $f_v$ are also decided by the magnitude of principal tensile strain and principal compressive strain.

b) Results of analysis

An analysis was conducted on specimen No. 1, whose design shear strength was $V_y$ = 15.1 tf ($V_{cd}$ = 8.21 tf, $V_{sd}$ = 6.87 tf) and was less than the flexural strength when calculated using the equations specified in "JSCE Concrete Specifications." Consequently, shear failure was expected to be predominant. Experimental and analytical results of stirrup strains showed good conformity, as shown in Fig. 17. Figure 18 gives the shear carried by the concrete and the stirrups. The shear carried by concrete, for example 16.8 tf when the shear force is 18.2 tf, is relatively high compared with the value calculated using the equation in "JSCE Concrete Specifications." Further, it can be seen from the figure that after the formation of shear cracks the shear resistance of concrete gradually decreases as applied shear force increases, and as a consequence the proportion of the shear borne by the concrete begins to fall. This is because the concrete gradually loses its ability to resist shear as cracks widen.

The specimen No. 1 failed finally in flexure with the maximum strain in the stirrups remaining at around 1000 $\mu$. This is probably because the concrete played a relatively large role in resisting the shear, as suggested by the analytical results using the Collins model.

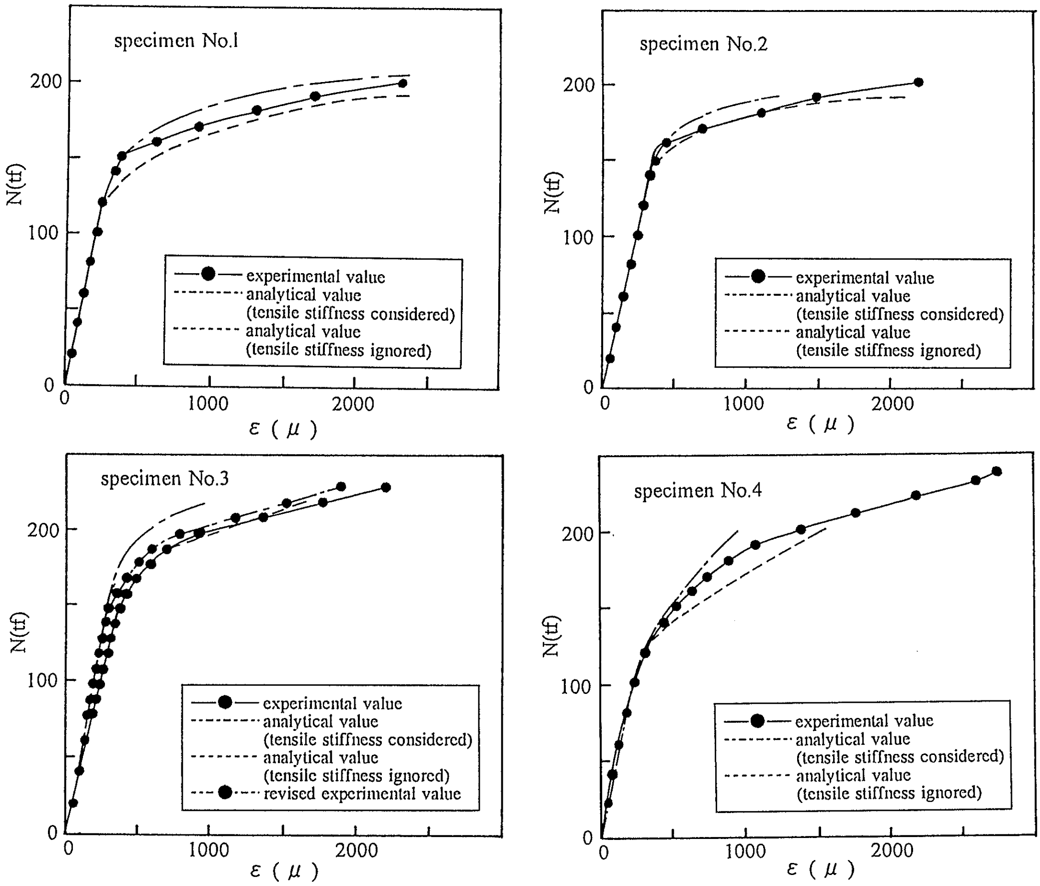


Fig.15 Relationship between axial force and strain of specimen

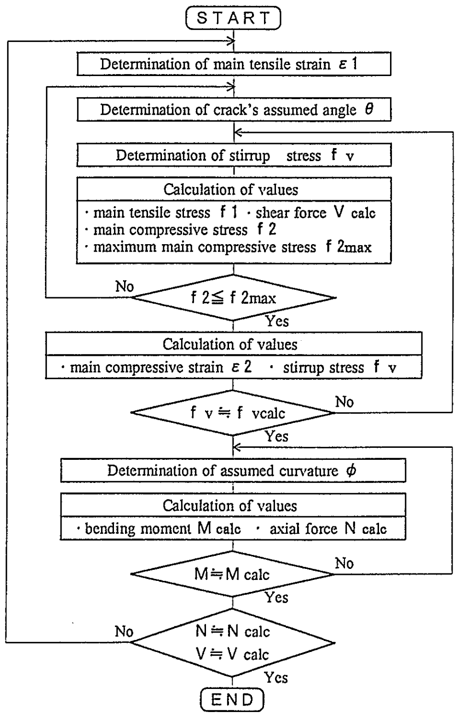


Fig. 16 Flowchart for analyzing shear strength

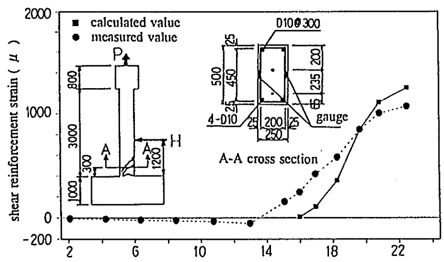


Fig. 17 Comparison of measured value and calculated value of shear reinforcement strain

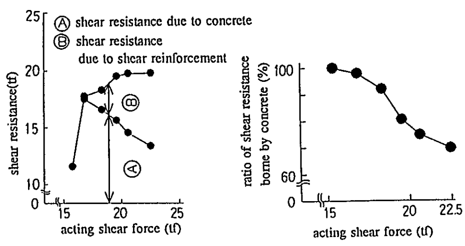


Fig. 18 Ratio of shear resistance shouldered by concrete and shear reinforcement

## 5. ANALYSIS OF BEARING CAPACITY OF THE ENTIRE BRIDGE STRUCTURE

### 5. 1 Outline of analysis

a) Model for analysis

The experimental results of the load carrying behavior under a combination of axial tensile force and bending moment showed that the ultimate strength can successfully be evaluated using an *N-M* interaction curve derived from the appropriate stress-strain characteristics of the constitutive materials, and that deformation in the axial direction can be accurately evaluated using a model that takes tensile stiffness of concrete into account. From these experimental results, we now use a plane frame model (the DIANA program) to extend the analysis over the entire structure of the bridge. And then, the results are compared with those of the linear analysis in Section 2. The model for analysis in this case is the entire structure of the three-span continuous bridge, as shown in Fig. 19. The area close to the intersection of a main pylon and a concrete stay is divided into smaller elements, as this area can be considered to have a large influence on the load bearing capacity of the structure. In each cross section, the prestressing steels and reinforcing bars are in the same arrangement as in an actual bridge, and prestress is introduced to prestressing steels as the initial strain.

b) Method of analysis

Members were divided into small elements both in the axial direction and in the direction perpendicular to the cross section of the members. Each element consist of concrete, reinforcing bars, and steels. Calculation was done by solving the stiffness equations of each element by load incrementing procedure based on the Newton-Raphson method. The stay members were divided into five elements in the axial direction, while in the direction perpendicular to the cross section, the members were divided into elements according to the member length considering the anticipated crack spacing and the plastic hinge range. The stress-stain relationship was calculated at the integral point of the elements, and determinations of cracking and yielding were also implemented at the same point. The stress-strain at the integration point, and the force and displacement at the nodal point were related to each other through compensating functions. The calculation procedure, as shown in the flow chart of Fig. 20, involved calculating the displacement using the initial stiffness, deriving the internal energy. If the discrepancy was judged major, the displacement was adjusted according to the magnitude of discrepancy. In other words, a shortfall in internal energy was compensated for by increasing or decreasing the strain, and convergence was repeatedly tested until the discrepancy fell within the tolerable range.

Selecting the design curve specified in "Specifications for Highway Bridges" of the many stress-strain curves of concrete available, the ultimate compressive strain was set to be 0.0035. As a stress-stain relation for the PC steel, a bilinear model was adopted with yield point ($\varepsilon py$ = 0.00805; $\sigma py$ = 16,100 kgf/cm$^2$ ) and an ultimate state ($\varepsilon pu$ = 0.067; $\sigma pu$ = 19,200 kgf/cm$^2$ ). The following three cases were compared in the analysis, with the effect of concrete tensile stiffness as a parameter: 1) stiffness beyond the concrete tensile strength ignored; 2) approximately half the tensile stiffness of the Collins model considered, so that concrete stress equals to zero in the strain softening range at a strain value corresponding to the yield stress of the reinforcing steels; 3) tensile stiffness according to the Collins model considered.

### 5.2 Results of analysis

The results of analysis for the three cases are given in Table 4. A typical N-M interaction curve taken from cross section No. 98 at the intersection of a stay and pylon is shown in Fig. 21. It is indicated in Table 4 that the most critical section in which PC members failed is, in all three cases, the section where a stay intersects a main pylon (cross section No. 98). Second critical is the section around the mid-point of the main girder (cross section No. 33), as predicted in the linear analysis. The bending moment commences to decrease with the increasing load after the formation of cracks, as is clear in Fig. 21. This is because a plastic hinge-like phenomenon occurs and resistance at the other sections increases, causing a redistribution of forces. Namely in case 1, the load factor is $\alpha = 6.9$, which gives a 30% increase in load bearing capacity compared with the results of linear analysis ($\alpha = 5.3$). Furthermore, case 2 ($\alpha = 7.8$) and case 3 ($\alpha = 8.6$), both of which take tensile stiffness into account, give a significant increase in load bearing capacity by about 50% and 60%, respectively, compared with the linear analysis.

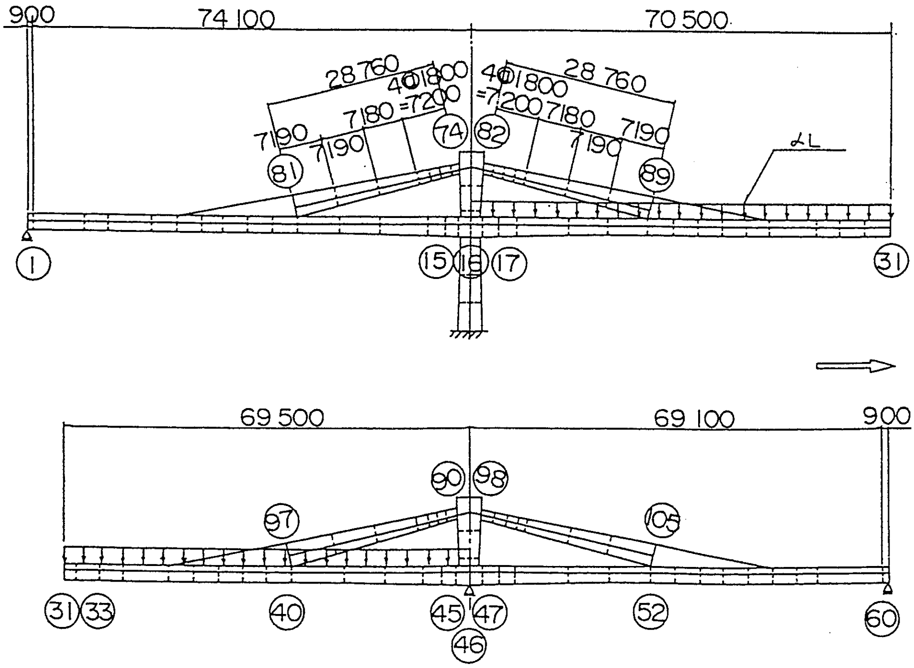


Fig.19 Model for analysis

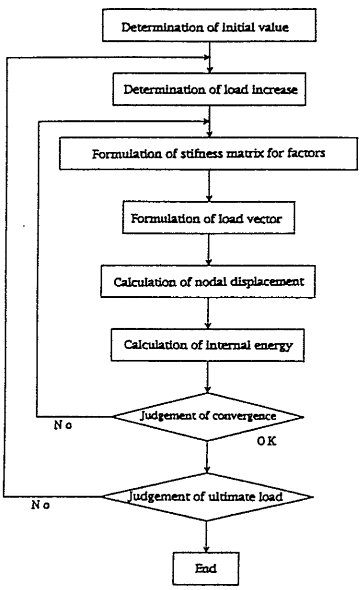


Fig. 20 Flowchart for analysis

| α | CASE−1 | CASE−2 | CASE−3 |
|---|---|---|---|
| 2.5 | crack developed at 90 cross section | crack developed at 90 cross section | crack developed at 90 cross section |
| 2.75 | crack developed at 33 cross section | crack developed at 33 cross section | crack developed at 33 cross section |
| 3.6 | crack developed at 98 cross section | | |
| 4.1 | | crack developed at 98 cross section | |
| 4.2 | | | crack developed at 98 cross section |
| 6.2 | | reinforcement yielded at 98 cross section | |
| 6.9 | ultimate state at 98 cross section | PC steel bar yielded at 33 cross section | |
| 7.2 | | | reinforcement yielded at 98 cross section |
| 7.7 | | | reinforcement yielded at 33 cross section |
| 7.8 | | ultimate state at 98 cross section | |
| 8.1 | | | PC steel bar yielded at 33 cross section |
| 8.7 | | | ultimate state at 98 cross section |

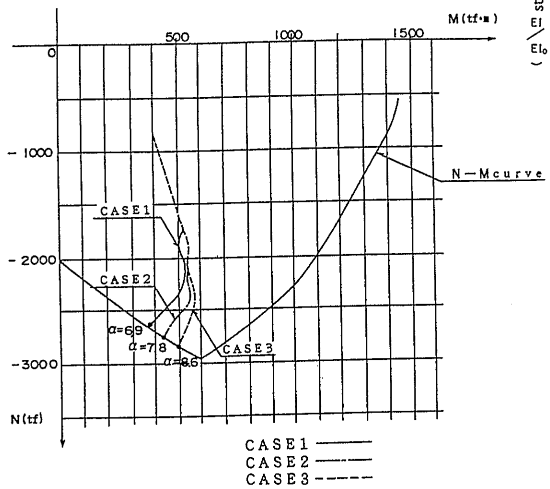


Fig.21 N-M curve at the intersection for diagonal stay and pylon

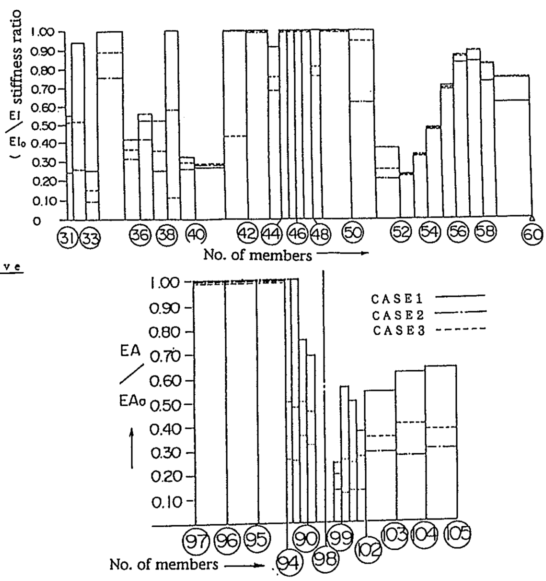


Fig.22 Decrease in stiffness

This is because, in addition to the redistribution effect, the load bearing capacity increase markedly as the tensile stiffness of the concrete increases, since the failure is governed by the resistance of the members to axial tensile force. As seen in Fig. 22, the decrease in tensile stiffness of the diagonal stays at the ultimate state is limited to the range 0.15 to 0.25 in case 1 to case 3. Also, the decrease in flexure stiffness of girders at the ultimate state is within the range 0.10 to 0.25. In all three cases, the intersection of a stay and a pylon reached the ultimate state first, followed by the girder mid-point.

## 6. CONCLUSION

Experimental and analytical investigations were conducted on a box girder bridge with prestressed concrete stays as prototype model structure. The following conclusions can be drawn regarding the load carrying and deformation behavior under a combination of axial tensile force and bending moment.

1) All of the five column specimens simulating PC stays which were produced with two parameters-- the shear reinforcement ratio and the combination of axial tensile force and bending moment (high axial force, low axial force, and axial force only) -- eventually exhibited flexural failure around the base of the column.

2) Analytical N-M relationships derived by taking into account the stress-strain properties of the constitutive members agreed relatively well with the experimental results in both the low axial force and high axial force loading patterns. Where only axial force was applied, a slight restraining moment occurred at the bottom end of the specimen, but the analytical result was in comparatively good accord with the experimental one as long as such restraining effect was duely considered.

3) The analytical results of $M$-$\phi$ relation for each specimen agreed relatively well with the experimental ones. Pull-out of steel reinforcement occurred around the bottom of the specimen had a conspicuous adverse effect on load bearing capacity as the load increased, so this is an important factor that must be given attention in evaluating the horizontal deformation behavior of the PC stay member.

4) Regarding the average strain in the axial direction of column specimens, the experimental results existed between two analytical results, one ignoring tensile stiffness of concrete and the other taking it into account based on the Collins model.
5) The analytical results for PC column members subjected to axial tensile force according to modified compression field theory showed fairly good agreement with the experimental ones as regards stirrup strain.
6) An analysis of the load carrying capacity of a PC box girder bridge with PC stays subjected to a live load indicated clearly that such a bridge has the ultimate load bearing capacity of 5.3 times the design capacity obtained from linear analysis, and 7.8 to 8.6 times the design capacity were obtained in nonlinear analysis taking tensile stiffness of concrete into consideration.
7) In a structure in which the axial tensile force plays a dominant role in bearing the load, the tension stiffening effect of concrete makes a comparatively significant contribution. Rational design will be made possible if this effect is appropriately taken into account in the nonlinear analysis of this type structures.

## Acknowledgements
The authors greatly appreciate the members of the concrete group of Hanshin Expressways' technical research committee (chairman: Prof. Manabu Fujii, Kyoto University) for their valuable advice in completing this paper. They are also indebted to Mr. Tadao Wakasa of New Structure Engineering, Inc. and Mr. Masato Koori of Tokyo Kensetsu Consultant, Inc. for their valuable assistance with both experiments and analysis.

## References
[1] Ueda, M. and Dobashi, Y. "Nonlinear Bond Slip Analysis of Axially Loaded Reinforced Concrete Prismatic Members," Proc. of JSCE No. 360, V-3, pp.71-80, 1985 (in Japanese)

[2] Yoshikawa, H., Hu, Z., and Tanabe T. "Numerical Investigation on the Nonlinear Behavior of Crack Surface in Concrete," Proc. of JSCE, No. 408, V-11, pp.71-80, 1989 (in Japanese)

[3] Collins, M.P. and Mitchell, D. , *Prestressed Concrete Structures,* Prentice Hall, 1991

[4] Tamai, S, Shima, H., Izumo, J., and Okamura, H., "Average Stress-Average Strain Relationship of Steel in Uniaxial Tension Member in Post-Yield Range," Proc. of JSCE, No. 378, V-6, pp.239-247, 1987 (in Japanese)

[5] Revised version of *Standard Specifications for Concrete* (1986), JSCE, pp.163-166, 1987.10 (in Japanese)

[6] Tamura, T., Shigematu, T., Hara, T., and Nakano, S., "Experimental Analysis of Shear Strength of Reinforced Concrete Beams Subjected to Axial Tension," Proc. of JCI. Vol. 2, No. 2. pp.153-160, 1991 (in Japanese)

[7] Vecchio, F.J., and Collins, M.P., "The Modified Compression-Field Theory for Reinforced Concrete Elements Subjected to Shear," *ACI Structural Journal,* pp.219-231, 1986

[8] *Specifications for Highway Bridges:III Concrete Bridges,* Japan Road Association, pp.116-126, 1991 (in Japanese)